Layer-specific analysis and spatial prediction of soil organic carbon using terrain attributes and erosion modeling

Verena Dlugoß, Peter Fiener, Karl Schneider

Angaben zur Veröffentlichung / Publication details:

Dlugoß, Verena, Peter Fiener, and Karl Schneider. 2010. "Layer-specific analysis and spatial prediction of soil organic carbon using terrain attributes and erosion modeling." *Soil Science Society of America Journal* 74 (3): 922–35. https://doi.org/10.2136/sssaj2009.0325.

Layer-Specific Analysis and Spatial Prediction of Soil Organic Carbon Using Terrain Attributes and Erosion Modeling

Verena Dlugoß
Peter Fiener*
Karl Schneider
Dep. of Geography
Univ. of Cologne
Albertus Magnus Platz
50923 Köln, Germany

High-resolution soil organic C (SOC) maps are a major prerequisite for many environmental studies dealing with C stocks and fluxes. Especially in hilly terrain, where SOC variability is most pronounced, high-quality data are rare and costly to obtain. In this study, factors and processes influencing the spatial distribution of SOC in three soil layers (<0.25, 0.25–0.50, and 0.5–0.90 m) in a sloped agricultural catchment (4.2 ha) were statistically analyzed, utilizing terrain parameters and results from water and tillage erosion modeling (with WaTEM/SEDEM). Significantly correlated parameters were used as covariables in regression kriging (RK) to improve SOC mapping for different input data densities (6–38 soil cores ha^{-1}) and compared with ordinary kriging (OK). In general, patterns of more complex parameters representing soil moisture and soil redistribution correlated highest with measured SOC patterns, and correlation coefficients increased with soil depth. Analogously, the relative improvement of SOC maps produced by RK increased with soil depth. Moreover, an increasing relative improvement of RK was achieved with decreasing input data density. Hence, the expected decline of interpolation quality with decreasing data density could be reduced, especially for the subsoil layers, by incorporating soil redistribution and wetness index patterns in RK. The optimal covariable differed among the soil layers. This indicates that bulk SOC patterns derived from topsoil SOC measurements might not be appropriate in sloped agricultural landscapes; however, generally more complex covariables, especially patterns of soil redistribution, exhibit a great potential to improve subsoil SOC mapping.

Abbreviations: CA, catchment area; C-plan, plan curvature; C-prof, profile curvature; DEM, digital elevation model; MEF, model-efficiency coefficient; OK, ordinary kriging; RE, relative elevation; RI, relative improvement; RK, regression kriging; RUSLE; Revised Universal Soil Loss Equation; R_{17}, 17-m input raster; R_{25}, 25-m input raster; R_{50}, 50-m input raster; SEDEM, Sediment Delivery Model; SOC, soil organic carbon; SPI, stream power index; WaTEM, Water and Tillage Erosion Model; WI, wetness index.

Soils play a major role in the global C cycle. Approximately 1500 Pg of C are stored in the topmost meter of soils worldwide, corresponding to twice the amount of atmospheric C and triple the amount of C stored in the biosphere (Schlesinger, 2005). Nevertheless, the role of this reservoir as a CO_2 sink or source in global climate and environmental studies is not clear. To analyze the possibilities of soils to sequester atmospheric CO_2, as well as for other environmental issues (e.g., analysis of soil quality and adaptation of management practices), detailed and precise maps of the distribution of SOC are an essential prerequisite. Especially in agricultural regions, the complex arrangement and combination of topography, soil, and management practices as well as the biological processes controlled by these parameters lead to a high spatial variability of SOC. A rolling topography also affects the spatial heterogeneity of SOC in agricultural fields through soil redistribution processes. Most studies dealing with soil and SOC redistribution indicate an increase of SOC in depositional areas, compared with regions of erosion, where SOC is depleted (e.g., Ritchie et al., 2007; Mabit et al., 2008); however, there are also opposite results published in literature. For example, Arriaga and Lowery (2005) found that the introduction of clayey subsoil material into the

plow layer due to erosion of the topsoil stabilized and hence increased the SOC content in the topsoil of severely eroded sites. Below the plow layer, a decrease in SOC occurred in areas of erosion, while more or less constant SOC contents were found throughout the soil profile in regions of soil deposition (Arriaga and Lowery, 2005).

To produce accurate SOC maps, in general, different kinds of interpolation schemes are applied based on point measurements. As field measurements are costly and time consuming, the improvement of interpolation methods to derive spatial SOC patterns using secondary information is important and has been extensively tested. Terrain attributes of various complexities have been used as proxies for relief-driven processes of pedogenesis. In most studies, primary terrain parameters, which can be easily derived from digital elevation models (DEMs), such as (relative) elevation (Mueller and Pierce, 2003; Ping and Dobermann, 2006; Sumfleth and Duttmann, 2008), slope (Mueller and Pierce, 2003; Ping and Dobermann, 2006; Takata et al., 2007; Sumfleth and Duttmann, 2008), aspect (Odeh et al., 1994, 1995), and curvature (Terra et al., 2004; Takata et al., 2007) were used as secondary information. These primary terrain parameters can also be combined, resulting in more complex secondary terrain parameters or indices comprising landscape processes more explicitly. Often the wetness (or topographic) index (Beven and Kirkby, 1979) has been tested for its capability to improve the interpolation of SOC and other soil properties (e.g., Herbst et al., 2006; Takata et al., 2007; Sumfleth and Duttmann, 2008). In addition to these terrain parameters, other parameters have also been used as covariables for interpolation schemes. Takata et al. (2007), for example, used the enhanced vegetation index, whereas Chen et al. (2000) used soil color to successfully predict the spatial distribution of SOC. Both parameters were derived from remote sensing data. Another covariable utilized effectively to improve the interpolation of SOC is the electrical conductivity of the topsoil layer (Terra et al., 2004; Simbahan et al., 2006; Ping and Dobermann, 2006).

A variety of statistical and geostatistical methods exist to interpolate point data with and without consideration of secondary information (e.g., Isaaks and Srivastava, 1989; Webster and Oliver, 2001). While simple statistical approaches to interpolate SOC, such as a (multiple) linear regression, performed well under certain circumstances (e.g., Mueller and Pierce, 2003), often geostatistical kriging approaches, which account for the spatial structure of SOC as well as that of covariables, performed better. Whereas ordinary kriging utilizes only the spatial autocorrelation of the target variable, there are several geostatistical techniques that allow the incorporation of a spatial trend caused by spatial patterns of secondary parameters in the kriging approach. Most often regression kriging (RK) or kriging with external drift (KED) has been applied. In contrast to KED, which is a one-algorithm system, RK is a stepwise approach combining a regression between the target and a covariable with simple or ordinary kriging of the regression residuals. Whereas the target and the covariable have to be linearly related in KED, RK also allows the integration of more complex regression models (i.e., multiple linear or nonlinear functions). Kriging with external drift and linear RK differ only in the computational steps used, but the resulting predictions are the same given the same input data (target and covariable) and the same regression fitting method (Hengl et al., 2007).

Odeh et al. (1994, 1995) defined three types of regression kriging, of which regression kriging Model C, where the trend function is calculated using ordinary least squares and the residuals are interpolated using ordinary kriging, was successfully used to improve the interpolation of SOC as well as that of other soil properties in many studies (e.g., Terra et al., 2004; Herbst et al., 2006; Takata et al., 2007; Sumfleth and Duttmann, 2008).

A geostatistically more sophisticated approach, which overcomes some statistical deficiencies of KED and RK, is REML-EBLUP (Lark et al., 2006). In this method, the trend model is estimated using residual maximum likelihood (REML), and subsequently the estimated parameters are used for the empirical best linear unbiased prediction (EBLUP). Minasny and McBratney (2007a,b), however, who compared RK Model C with REML-EBLUP for interpolating four different soil properties, concluded that, although statistically somewhat inappropriate, RK has proven to be a robust technique for practical applications. In concordance with these results, Chai et al. (2008), who analyzed the effect of different covariables on the spatial interpolation of soil organic matter, concluded that REML-EBLUP was more stable, but that the improvement was not significant compared with RK.

To our knowledge, all studies that have explicitly dealt with the interpolation of SOC and its possible improvement by incorporating covariables in the interpolation process have focused on the topsoil layer (<0.3 m, e.g., Mueller and Pierce, 2003; Terra et al., 2004; Simbahan et al., 2006; Ping and Dobermann, 2006; Takata et al., 2007; Sumfleth and Duttmann, 2008); however, the spatial patterns of SOC in sloped agricultural catchments might differ substantially in different soil depths. This aspect should be taken into account for studies addressing the soil C balance as well as for simulations of soil C dynamics.

The objectives of this study were: (i) to evaluate the spatial patterns of SOC for different soil layers in a small agricultural catchment and to analyze their relation to spatial patterns of terrain parameters and the results from soil redistribution modeling, and (ii) to evaluate whether these (easily available) parameters can serve as improving covariables in a layer-specific interpolation of SOC data by RK, and hence potentially allow a reduction in SOC sampling density without a loss of mapping quality.

MATERIALS AND METHODS

Test Site

The test site is part of the Pleiser Hügelland, a hilly landscape located about 30 km southeast of Cologne in North Rhine-Westphalia, Germany. It covers a small catchment of approximately 4.2 ha at an altitude of 125 to 154 m above sea level (Fig. 1) that is part of a larger agricultural field (50°43′ N, 7°12′ E). Slopes range from 1° in the west up to 9° in the eastern part with a relatively flat thalweg area heading to the outlet.

The mean annual air temperature is 10.0°C and the average precipitation per year is 765 mm (1990–2006), with the highest rainfall intensities occurring from May to October (data from the German Weather Service station at Bonn-Roleber, located about 1 km to the west of the test site, 159 m above sea level).

Due to its fertile, loess-containing, silty and silt-loamy soils classified as Alfisols (Soil Survey Staff, 1999) and its proximity to the agglomeration of Cologne-Bonn, the test site is used intensively for arable agriculture. The present crop rotation consists of sugarbeet (*Beta vulgaris* L.), winter wheat (*Triticum aestivum* L.), and winter barley (*Hordeum vulgare* L.). Since 1980, a no-till system has been established with mustard (*Sinapis arvensis* L.) cultivated as a cover crop after winter barley.

Soil Sampling and Soil Organic Carbon Measurement

To investigate the vertical and horizontal distribution of SOC in the test site, a first set of soil samples was taken in April 2006. It consisted of 92 soil cores, of which 71 cores were positioned on a regular 25- by 25-m raster. To account for small-scale spatial variability of SOC, additionally a north–south transect in the eastern part of the test site with point distances of 12.5 m and two microplots consisting of nine sample points each in a 1- by 1-m raster were augered. In each of the microplots, the central sampling point belonged to the regular 25- by 25-m raster. Microplots were selected to cover different slope positions. To increase the density of the first sampling grid, a second set of soil cores ($n = 65$) was taken in March 2007 using a 25- by 25-m raster that was offset by 12.5 m to the north and west in relation to the 2006 raster. Additionally, three samples were taken near the outlet of the test site to account for a small colluvial area. Thus, soil samples are available in a regular 17.7- by 17.7-m raster with a density of 38 samples ha^{-1} (Fig. 1), with additional samples along the transect and in the microplots. Within each sampling campaign, soil cores were extracted with a Pyrckhauer soil auger (approximately 2-cm diameter) and soil samples were taken in three depths (I: 0–0.25 m; II: 0.25–0.50 m; III: 0.50–0.90 m). All sampling points were surveyed with a differential global positioning system with a horizontal accuracy between 0.5 and 2.0 m.

After oven drying at 105°C for 24 h, the samples were ground and coarse particles were separated by 2-mm sieving. Roots and other recognizable undecomposed organic matter particles were removed by hand picking. The total C content was determined by dry combustion using a CNS elemental analyzer (Vario EL, Elementar, Hanau, Germany). Although loess soils in the area are in most cases deeply decalcified, all soil samples were checked for lime ($CaCO_3$) with HCl (10%). If any inorganic C content was recognized, its amount was determined according to the Scheibler method (Deutsches Institut für Normung, 1996). Combining both methods if necessary, the SOC content was calculated from total minus inorganic C.

Terrain Analysis

A set of primary terrain attributes and secondary terrain indices that might have affected the spatial distribution of SOC was calculated. The indices combine different primary terrain attributes and thus represent landscape processes more explicitly. The derivation of these parameters was based on a DEM with a 6.25- by 6.25-m grid. The DEM was interpolated from Lidar data (2–3-m point distance) provided by

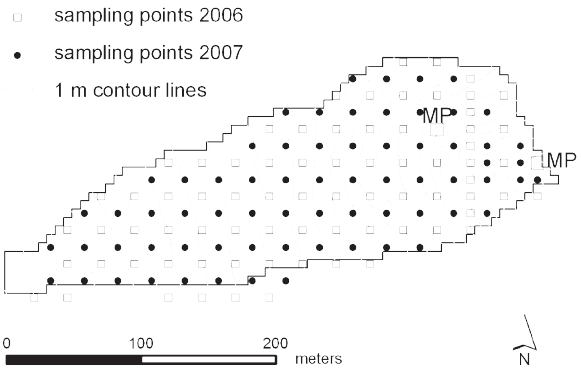

Fig. 1. Test site with location of soil sampling points. Each of the two microplots (MP) consists of nine sample points arranged in a 1- by 1-m grid; flow direction is from west to east.

the Landesvermessungsamt North Rhine-Westphalia using ordinary kriging (spherical model; nugget: 0.6; sill: 46.2; range: 237 m) within the Geostatistical Analyst of the geographic information system ArcGis 9.2 (ESRI, Redlands, CA). A grid size of 6.25 by 6.25 m was chosen to assure that each sampling point was located in the center of a grid cell.

The following primary terrain attributes were calculated using ArcGis 9.2: the relative elevation (RE), which is the vertical distance of every grid cell to the outlet of the catchment, the slope, the aspect, and the curvature. The curvature is the second derivative of the surface and is separated into profile curvature (C-prof, the curvature in the direction of maximum slope) and plan curvature (C-plan, the curvature perpendicular to the direction of maximum slope). Another primary terrain attribute used in this study is the catchment area, CA, calculated for each grid cell using the extension HydroTools 1.0 for ArcView 3.x (Schäuble, 2004). The multiple flow algorithm of Quinn et al. (1991) was applied, in which the flow is distributed among three downslope grid cells weighted by slope gradient. The catchment area takes into consideration the amount of surface water that is distributed toward each grid cell. The parameter thus is related to soil moisture and infiltration as well as erosion and deposition. The two combined indices, wetness index (WI) and stream power index (SPI), differentiate between these two process groups more explicitly through the incorporation of the local slope gradient. The WI characterizes the distribution of zones of surface saturation and soil water content in landscapes (Beven and Kirkby, 1979) and is calculated as

$$WI = \ln \frac{SCA}{\tan S} \quad [1]$$

where SCA is the specific catchment or contributing area ($m^2\ m^{-1}$) orthogonal to the flow direction and is calculated as the CA divided by the grid length (6.25 m) and S is the slope (°).

The SPI is the product of the specific catchment area, SCA ($m^2\ m^{-1}$), and slope S (°) (Moore et al., 1993):

$$SPI = SCA \tan S \quad [2]$$

It is directly proportional to stream power and can thus be interpreted as the erosion disposition of overland flow.

Erosion Modeling

To more explicitly consider different soil redistribution processes due to water (E_{wat}), tillage (E_{til}), and total (E_{tot}) erosion and deposition, corresponding patterns were calculated by applying the long-term soil erosion and sediment delivery model WaTEM/SEDEM version 2.1.0 (Van Oost et al., 2000; Van Rompaey et al., 2001; Verstraeten et al., 2002).

The WaTEM/SEDEM model is a spatially distributed model combining WaTEM (Water and Tillage Erosion Model) (Van Oost et al., 2000) and SEDEM (Sediment Delivery Model) (Van Rompaey et al., 2001). The WaTEM model consists of water and tillage erosion components that can be run separately. The water erosion component uses an adapted version of the Revised Universal Soil Loss Equation (RUSLE, Renard et al., 1996). Adaptations consist in the substitution of slope length with the unit contributing area calculated following Desmet and Govers (1996) and the integration of sedimentation following an approach of Govers et al. (1993). Tillage erosion is caused by variations in tillage translocations across a landscape and always results in a net soil displacement in the downslope direction. The net downslope flux, Q_{til} (kg m^{-1} yr^{-1}), due to tillage implementations on a hillslope of infinitesimal length and unit width is calculated with a diffusion-type equation adopted from Govers et al. (1994) and is proportional to the local slope gradient:

$$Q_{til} = k_{til} S = -k_{til} \frac{dH}{dx} \quad [3]$$

where k_{til} is the tillage transport coefficient (kg m^{-1} yr^{-1}), S is the local slope gradient (%), H is the height at a given point of the hillslope (m), and x the distance in the horizontal direction (m). The local erosion or deposition rate, E_{til} (kg m^{-2} yr^{-1}), is then calculated as

$$E_{til} = -\frac{dQ_{til}}{dx} = \frac{d^2H}{d^2x} \quad [4]$$

Because tillage erosion is controlled by the change in the slope gradient and not by the slope gradient itself, erosion takes place on convexities and soil is accumulated in concavities. The intensity of the process is determined by the constant k_{til}, which ranges between 500 and 1000 kg m^{-1} yr^{-1} in western Europe (Van Oost et al., 2000).

A second module of WaTEM/SEDEM calculates sediment transport and sedimentation. The sediment flow pattern is calculated with a multiple flow algorithm (Desmet and Govers, 1996). The sediment is routed along this flow pattern toward the river, taking into account its possible deposition. Deposition is controlled by the transport capacity computed for each grid cell. The transport capacity is the maximal amount of sediment that can pass through a grid cell and is assumed to be proportional to the potential rill (and ephemeral gully) erosion volume (Van Rompaey et al., 2001). If the local transport capacity is lower than the sediment flux, deposition is modeled.

The WaTEM/SEDEM model requires the input of several maps as well as various constants and was implemented as follows: The 6.25- by 6.25-m DEM served as the basis for the calculations. Additionally, a land use map containing field boundaries and was derived from digital aerial photographs provided by the Landesvermessungsamt North Rhine-Westphalia. The K factor of the RUSLE was also given as a map with values ranging from 0.058 to 0.061 kg h m^{-2} N^{-1}. This map was derived from a digital soil map (1:50,000 scale) provided by the Geological Survey of North Rhine-Westphalia. Accounting for the crop rotation and the implemented soil conservation practice at the test site, the C factor was set to 0.05 (Deutsches Institut für Normung, 2005). The R factor of the USLE was calculated with a regression equation between R factor and mean summer precipitation developed for North Rhine-Westphalia (Deutsches Institut für Normung, 2005). Therefore, precipitation data (1990–2006) of the German Weather Service station at Bonn-Roleber were used, resulting in an R factor of 67 N h^{-1} yr^{-1}. Since no sediment yield data for model calibration were available, modeling was first performed on a 20- by 20-m grid, which is the grid size used in earlier, calibrated simulations under similar environmental conditions in the Belgium Loess Belt (Verstraeten et al., 2006). The results of this first simulation were used to recalibrate the transport capacity coefficients to run the model on a 6.25- by 6.25-m grid. All other constants necessary for running WaTEM/SEDEM were set to default because no absolute but only relative erosion and deposition values were needed.

Statistical and Geostatistical Analyses

Statistical Analysis

For statistical and geostatistical analyses, three SOC input grids with different sampling densities were created. To achieve a dense 17.7- by 17.7-m sample raster (R_{17}), SOC data of the 2006 and 2007 sampling campaign were combined in each soil layer. For the topsoil layer, it was assumed that interannual differences of sampling date and thus of planted crops, soil management, and climate could have resulted in differences in SOC concentrations as measured during the two sampling campaigns. Thus, after assessing normal distribution by analyzing skewness coefficients, a Student's t-test (although not optimal when used with spatially autocorrelated data) was applied to estimate the equality of means of the SOC data of the two sampling years. In the two deeper soil layers, these influences were considered negligible. There, the SOC contents of the two sampling dates were simply combined into one data set. The 2006 sampling points (n = 92) arranged in a 25-m raster (R_{25}) served as an input data set with a medium density of 17 samples ha^{-1} for each soil layer. To produce a low-density, 50-m input raster (R_{50}, n = 44), every second data point of R_{25} was eliminated, resulting in a density of approximately 6 samples ha^{-1}. Each raster contained the transect and the two microplots to include short distances in the geostatistics.

The relationship between the spatial patterns of SOC and the spatial patterns of potential covariables was tested using Pearson correlation coefficients calculated between all parameters and the SOC data for each soil layer and each raster width. In this correlation analysis, the eight additional points of the microplots were excluded because all nine sampling points of a microplot were located in one grid cell with one value for the relevant parameter. Parameters that were significantly (P < 0.05) related to SOC in a soil layer were tested for their potential to improve the interpolation results when used as a linear trend in RK.

Geostatistical Analysis

Geostatistical methods are based on the theory of regionalized variables (Matheron, 1963). For further information concerning the

theoretical background of geostatistics, see Isaaks and Srivastava (1989) or Webster and Oliver (2001). The basic assumption is that sample points located close to each other are more similar than sample points farther apart. This spatial autocorrelation is quantified in an empirical semivariogram of the sampled data, where the semivariance is plotted as a function of the lag distance. For a data set $z(x_i)$, $i = 1, 2, ...$, the semivariance g of a certain lag distance h is calculated as

$$\gamma(h)=\frac{1}{2n(h)}\sum_{i=1}^{n(h)}\left[z(x_i)-z(x_i+h)\right]^2 \qquad [5]$$

where $n(h)$ is the number of pairs of data points separated by lag h, and $\gamma(h)$ is the semivariance of a certain lag distance h. To apply this semivariogram in the following interpolation process, known as *kriging* in geostatistics, a theoretical model has to be fit to the sample variogram.

Ordinary kriging (OK) which only uses the spatial autocorrelation of the target variable can be considered as a basic geostatistical interpolation method. It can be described as a weighted spatial mean, where sample point values x_j are weighted according to the semivariance as a function of distance to the prediction location x_0. The weights λ_i are chosen by solving the OK system to minimize the kriging variance:

$$\begin{aligned}&\sum_{i=1}^{n}\lambda_i\gamma(x_i,x_j)+\varphi=\gamma(x_i,x_0)\\&\sum_{i=1}^{n}\lambda_i=1\end{aligned} \qquad [6]$$

where $\gamma(x_i,x_j)$ is the semivariance between the sampling points x_i and x_j, $\gamma(x_i,x_0)$ is the semivariance between the sampling point x_i and the target point x_0, and φ is a Lagrange multiplier necessary for the minimization process (Ahmed and De Marsily, 1987).

The regression kriging used in this study follows regression kriging Model C described in Odeh et al. (1995) and accounts for a possible trend in the data combining linear regression with OK of the residuals. In a first step, a linear regression function of the target variable with the covariables is used to create a spatial prediction of the target variable at the new locations. In a second step, OK is applied to the residuals of the regression, resulting in a spatial prediction of the residuals. Finally, the spatially distributed regression results and the kriged residuals are added to calculate the target variable at all new locations.

As a prerequisite of geostatistics, the SOC data in each soil layer and in each raster width should be normally distributed. Following Kerry and Oliver (2007a), this prerequisite can be met in geostatistical analysis if the absolute skewness coefficient (SC) is <1. Moreover, data with an asymmetry caused by aggregated outliers need not to be transformed if the absolute SC is <2 (Kerry and Oliver, 2007b). If this was true, the SOC data were not transformed. For use in RK, the residuals resulting from linear regression with the significantly correlated parameters in each soil layer and in each raster width should also be normally distributed. Skewness coefficients as well as normal Q–Q plots of the residuals were analyzed. If the residuals showed strong deviations from a normal distribution, the corresponding parameters were logarithmically transformed and a linear regression analysis was applied (these transformed covariables are indicated by the subscript *tr*).

For each raster width and each of the three soil layers, SOC was interpolated using OK and RK with the selected parameters as covariables to target points spanning a 6.25- by 6.25-m raster within the test site. For the construction of omnidirectional empirical semivariograms of the original SOC data as well as of the residuals, the maximum distance up to which point pairs were included was set to 200 m, which is half of the maximum extent of the test site in the east–west direction. Lag increments were set to 10 m. In each approach, two theoretical variogram models (exponential and spherical) and three methods for fitting the variogram model to the empirical variogram, including ordinary least squares (i.e., equal weights to all semivariances) and two weighted least square methods (weighting by n_p = number of pairs and weighting by $n_p h^{-2}$ with h = lag distance), were applied. To evaluate the various theoretical variograms against the original data and to choose the best model, a cross-validation procedure was implemented. In the cross-validation procedure, one measurement was omitted in the variogram construction, this value was subsequently estimated by the kriging (OK and RK) method, and the estimate was finally compared with the measurement. This procedure was applied to all measurements one at a time.

As a measure of spatial dependence, the ratio of the nugget to the sill (%) was calculated reflecting the influence of the random component to the spatial variability. Following Cambardella et al. (1994) nugget/sill ratios between 0 and 25% show that the data are highly spatially structured with low nugget variances, whereas ratios between 25 and 75% indicate moderate spatial dependence. Data with ratios >75% are weakly spatially structured, with a high proportion of unexplained variability.

Validation

The previously described cross-validation procedure was also used to validate the kriging results of the high-density input grid (R_{17}) and to compare the performance of the different geostatistical approaches in this raster width, although it systematically underestimates the quality of predictions when using a regular input grid (Isaaks and Srivastava, 1989; Mueller et al., 2001, 2004). Nevertheless, we used this procedure to avoid a loss of information in the input data. When using the reduced sampling grids R_{25} or R_{50} as input data, the 2007 sampling points ($n = 67$) were used for validation and for comparing the different kriging approaches within each raster width. Analogously to the cross-validation procedure, this procedure also underestimates the prediction quality because the tested prediction distance is much larger than the requested prediction distance of the resulting SOC maps. Hence, the measures of goodness-of-fit can be regarded as somewhat conservative. Because the main objective of this study was to analyze whether the prediction precision can be improved within one raster width when incorporating secondary parameters in the kriging process, however, this validation method can be accepted as a suitable approach.

Because different validation schemes had to be applied for the three input data sets due to the lack of an independent and randomized validation data set, a direct quantitative comparison of the interpolation results obtained for R_{17} and the two reduced input data sets is not possible. Comparisons of the different raster widths can only be done in qualitative terms.

To evaluate the goodness-of-fit of the various kriging results, a set of indices was used. To account for the bias and the precision of the prediction, the mean error (ME) and the root mean square error (RMSE) were calculated:

$$\mathrm{ME}=\frac{1}{n}\sum_{i=1}^{n}z(x_i)-\hat{z}(x_i) \quad [7]$$

$$\mathrm{RMSE}=\sqrt{\frac{1}{n}\sum_{i=1}^{n}\left[z(x_i)-\hat{z}(x_i)\right]^2} \quad [8]$$

where n is the number of points in the validation sample or the number of points used for cross-validation, $z(x_i)$ is the observed values, and $\hat{z}(x_i)$ is the predicted values. The ME should be close to zero for unbiased predictions, and the RMSE should be as small as possible. Additionally, the model-efficiency coefficient (MEF) of Nash and Sutcliffe (1970) was calculated:

$$\mathrm{MEF}=1-\frac{\sum_{i=1}^{n}\left[z(x_i)-\hat{z}(x_i)\right]^2}{\sum_{i=1}^{n}\left[z(x_i)-\overline{x}\right]^2} \quad [9]$$

The MEF is a measure of the mean squared error to the observed variance and ranges between $-\infty$ and 1. If the value of MEF = 1, the model or interpolation represents a perfect fit. If the error is in the same order of magnitude as the observed variance (MEF = 0), the arithmetic mean $\overline{x}$ of the observed values can represent the data as good as the interpolation.

The relative improvement, RI (%), of the prediction precision of RK with the selected covariables compared with OK was derived as

$$\mathrm{RI}=\frac{\mathrm{RMSE}_{\mathrm{OK}}-\mathrm{RMSE}_{\mathrm{RK}}}{\mathrm{RMSE}_{\mathrm{OK}}}100 \quad [10]$$

where $\mathrm{RMSE}_{\mathrm{RK}}$ and $\mathrm{RMSE}_{\mathrm{OK}}$ are the root mean square errors for a certain regression kriging approach and for ordinary kriging, respectively.

Additionally, the prediction quality was assessed by visual examination of the plots of predicted vs. measured SOC contents of the different kriging approaches. High quality results when the scatter of data or its linear regression fit adheres closely to the 1:1 line (Mueller et al., 2004).

The statistical and geostatistical analyses were performed with GNU R version 2.6 (R Development Core Team, 2007) and the supplementary geostatistical package gstat (Pebesma, 2004).

Table 1. Statistics of soil organic C content (% w/w) for 2006 and 2007 and the merged data set for three soil depths (I: 0–0.25 m; II: 0.25–0.50 m; III: 0.50–0.90 m).

Soil layer	Data set	n†	Soil organic C content						
			Mean	Median	SD†	CV†	Min.	Max.	SC†
			% (w/w)			%	% (w/w)		
I	2006	92	1.16	1.14	0.18	15.13	0.68	1.68	0.75
II	2006	92	0.67	0.67	0.22	32.62	0.13	1.19	0.24
III	2006	92	0.32	0.24	0.18	62.13	0.05	0.90	1.51
I	2007	67	1.11	1.08	0.16	12.23	0.85	1.43	0.30
II	2007	68	0.75	0.77	0.23	30.44	0.18	1.18	-0.32
III	2007	68	0.36	0.33	0.22	62.55	0.04	1.18	1.57
I	merged	159	1.14	1.12	0.17	14.91	0.68	1.68	0.74
II	merged	160	0.71	0.71	0.22	30.99	0.13	1.19	0.01
III	merged	160	0.34	0.27	0.21	62.61	0.04	1.18	1.50

† *n*, sample size; SD, standard deviation, CV, coefficient of variation; SC, Skewness coefficient.

RESULTS AND DISCUSSION

Measured Horizontal and Vertical Soil Organic Carbon Distribution

Because Student's *t*-test clearly shows that the SOC contents of the two sampling dates in Soil Layer I belong to the same population, SOC contents in each soil layer were combined into one data set. After merging the data sets, the SOC values in Soil Layer I ranged from 0.68 to 1.67% (w/w), in Soil Layer II from 0.13 to 1.19% (w/w), and in Soil Layer III from 0.04 to 1.18% (w/w) (Table 1). Maximum values in all soil layers were found in the flat area near the outlet of the test site (Fig. 2), indicating accumulation of SOC by depositional processes. This phenomenon is more pronounced with increasing soil depth. Another small area of relatively high SOC concentrations primarily in the two upper soil layers is located in the upper part near the southern boundary of the test site. We assumed that this was caused by areas formerly used for dung or sugarbeet storage, but no detailed data to verify or falsify this assumption regarding its location exist. Remarkably, the SOC distribution of the middle soil layer shows more small-scale variability than the other two soil layers. This indicates a small-scale change in the depth of the boundary between the topsoil with high SOC concentrations and the subsoil with lower SOC concentrations relative to the surface, which can be ascribed to soil redistribution processes. The results show that the majority of these transitions take place in this middle soil layer.

The maps of the measured SOC content (Fig. 2) show a decrease in SOC content and an increase in spatial variability with increasing soil depth, also indicated by increasing coefficient of variations (Table 1). The low spatial variability in Soil Layer I can be attributed to homogenization caused by management practices as well as to high turnover rates of soil organic matter in this soil layer. In the deepest soil layer, high SOC contents are most pronounced in the depositional area near the outlet of the test site, resulting in a SC of 1.5, indicating a non-normal distribution. Since this non-normality was caused by outliers aggregated in the depositional area (Fig. 2), the data were not transformed before further geostatistical analysis.

In general, the results show that the spatial patterns of SOC contents in the three soil layers differ substantially. This suggests that an evaluation of total SOC pools in a hilly agricultural terrain may fail if SOC analysis is restricted to the topsoil layer.

Terrain Parameters and Patterns of Soil Redistribution

Statistics and spatial patterns of the calculated terrain and soil redistribution parameters are shown in Table 2 and Fig. 3. All possible covariables have a considerable spatial variability within the test site, indicating their appropriateness for use in RK. The relative elevation, RE, has a clear tendency from west to east, with a maximum value of 27.4 m at the western boundary of the test site and a minimum of 0 m at the outlet. The slope shows a more complex pattern:

almost two-thirds of the test site (middle to western part) is relatively flat, with slopes ranging between 1 and 2°. Steep slopes (up to approximately 9.5°) exist in the eastern part. Incorporated into this easterly part is a very small thalweg area with still greater slopes (3–5°) than the flat westerly part. The spatial distribution of the aspect indicates the differentiation between a south-facing (values >135°) and a north-facing slope (values <45°) in the east. The flat westerly part is orientated to the east, with aspects ranging from approximately 60 to 120°. Profile and plan curvature show a diffuse behavior in the flat west, whereas the pattern of convexities and concavities in the east corresponds well to the derived slope pattern. The catchment area, CA, and the two indices WI and SPI are distributed in similar patterns, with a concentrated area of high values near the outlet of the test site. Compared with SPI, this area is smaller in the north–south direction and more elongated in the east–west direction in the patterns of CA and WI.

Comparing the distributions of tillage and water erosion (E_{til} and E_{wat}) derived from WaTEM/SEDEM clearly shows different spatial patterns of erosion and deposition resulting from these two processes, which agrees well with other studies (Govers et al., 1994; Van Oost et al., 2000). Areas with the steepest slopes have the highest water-induced erosion rates, resulting in an aggregated area of high erosion rates with values between -1.5 and -5.8 mm yr^{-1} in the test site. This aggregated area corresponds well to the areas with high values of SPI, indicating that these parameters represent similar processes. The rest of the test site is dominated by only slight water-induced erosion rates, with values between -1 and 0 mm yr^{-1}. No water-induced deposition was calculated inside the test site because WaTEM/SEDEM is not capable of modeling the backwater effect induced by the land use change at the outlet of the test site. Tillage-induced erosion generally occurs on convexities and on the downslope side of field boundaries, whereas deposition occurs on concavities, and on the upslope side of field boundaries (Govers et al., 1994; Van Oost et al., 2000). High tillage-induced deposition rates, with values ranging from 2 up to 15 mm yr^{-1}, were simulated in the thalweg area near the outlet of the test site, whereas highest erosion rates (-0.5 to -3 mm yr^{-1}) were simulated on the shoulders of the north–south-facing slope in the easterly part. The most pronounced difference between water and tillage erosion patterns were modeled along the thalweg: here deposition by tillage interacts with water-induced erosion. The pattern of total erosion (E_{tot}) combines the two soil redistribution patterns. Most grid cells experiencing tillage-induced deposition in the thalweg area are deposition sites in the total erosion pattern.

Relation between Soil Organic Carbon and Secondary Parameters

Among the primary terrain attributes, C-prof, C-plan, and CA showed significant linear relationships with SOC in all soil layers and in all input raster widths (Table 3). Correlation coefficients with C-prof and CA were always positive, whereas correlations with C-plan were always negative. Additionally, RE showed negative correlations with SOC in Soil Layer III for all

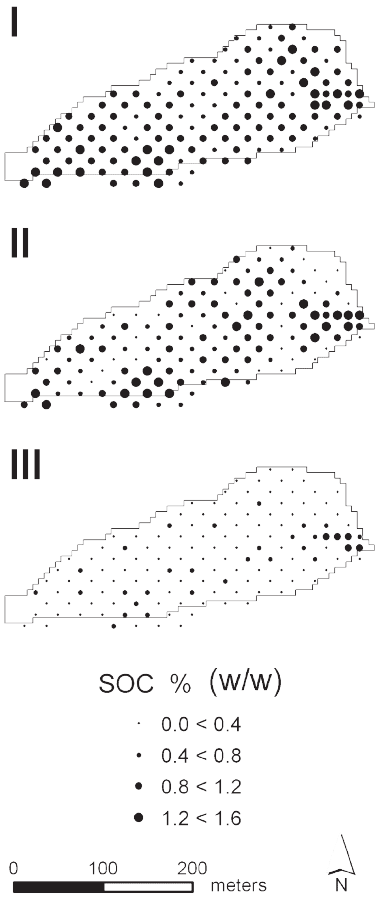

Fig. 2. Measured SOC contents at the 17.7- by 17.7-m raster sampling points for Soil Layers I (0–0.25 m), II (0.25–0.50 m), and III (0.50–0.90 m).

raster widths. The SPI and the soil redistribution patterns based on water and tillage erosion modeling all significantly correlated with SOC in all soil layers and in all raster widths, whereas the WI was only significantly correlated with SOC in the two subsoil layers. Correlations between SOC and E_{til} and E_{tot} were

Table 2. Statistics of terrain attributes and soil redistribution parameters within the test site (n = 1030): relative elevation (RE), slope, aspect, profile and plan curvature (C-prof and C-plan, respectively), catchment area (CA), wetness index (WI), stream power index (SPI), and patterns of tillage (E_{til}), water (E_{wat}), and total (E_{tot}) erosion.

Parameter	Mean	Median	SD	CV†	Min.	Max.	SC‡
RE, m	15.82	16.44	5.97	—	0.00	27.42	-0.31
Slope, °	3.93	3.21	1.87	47.58	1.56	9.46	1.05
Aspect, °	87.33	78.82	28.17	32.26	40.37	166.38	1.23
C-prof, 0.01 m	-0.03	-0.02	0.20	—	-1.08	0.95	-0.10
C-plan, 0.01 m	-0.04	-0.01	0.26	—	-1.27	0.72	-1.05
CA, m^2	1569	868	2635	168	105	25612	5.45
WI	7.79	7.90	0.90	—	5.73	11.00	-0.03
SPI	20.67	7.15	41.19	199.27	0.68	325.99	4.28
E_{til}, mm yr^{-1}	0.02	-0.16	1.49	—	-5.28	15.00	2.96
E_{wat}, mm yr^{-1}	-0.50	-0.23	0.66	—	-5.81	-0.02	-3.58
E_{tot}, mm yr^{-1}	-0.47	-0.44	1.30	—	-5.39	13.19	1.82

† The coefficient of variation cannot be calculated for variables containing negative values or possessing a negative skewness coefficient (Isaaks and Srivastava, 1989).

‡ Skewness coefficient.

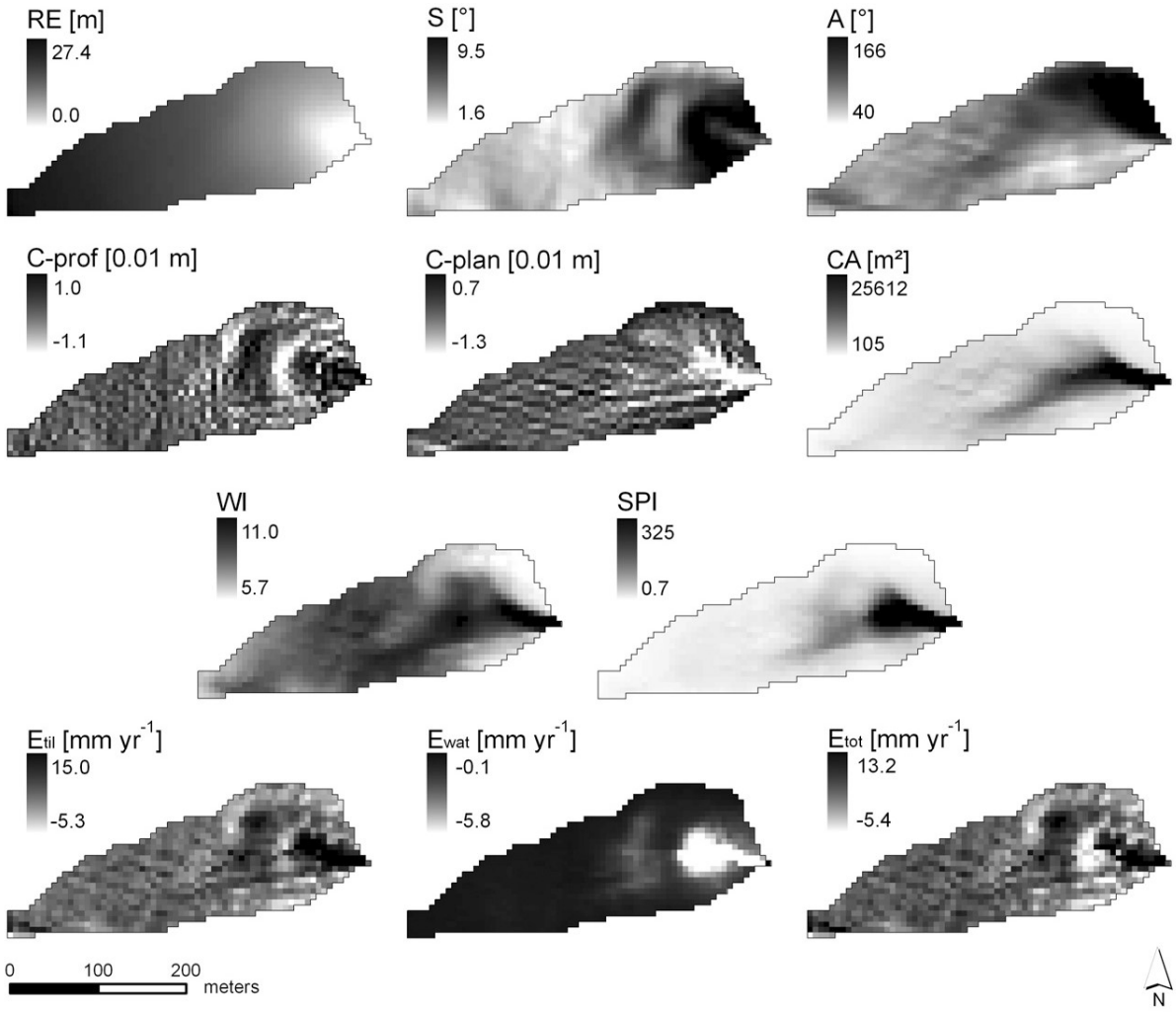

Fig. 3. Maps of terrain attributes and patterns of soil redistribution derived from the model WaTEM/SEDEM: relative elevation (RE), slope (S), aspect (A), profile and plan curvature (C-prof and C-plan, respectively), catchment area (CA), wetness index (WI), stream power index (SPI), and patterns of tillage (E_{til}), water (E_{wat}), and total (E_{tot}) erosion. A positive curvature (C-prof and C-plan) indicates that the surface is upwardly convex, and a negative value indicates that the surface is upwardly concave; negative values of E_{til}, E_{wat}, and E_{tot} represent erosion while positive ones represent deposition.

positive in each soil layer and in each raster width, indicating an accumulation of SOC at depositional sites and a loss of SOC at eroding sites. In contrast, the water-induced erosion pattern expressed by E_{wat} and SPI resulted in a different picture: high erosion rates corresponding to high SOC concentrations in each soil layer. This resulted from the counterbalancing effect of water and tillage erosion, which in most cases led to a net deposition considering both processes (see E_{tot}), while water erosion alone led to net erosion. Hence, it is misleading to use water erosion or corresponding indices alone as a covariable for any SOC interpolation scheme in agricultural landscapes.

In general, the linear relationship between SOC and the two indices, as well as between SOC and the erosion–deposition patterns, increased with increasing soil depth within each raster width. The same is true for the relationship between SOC and CA. This indicates (i) that relief-driven processes play a less significant role in the topsoil layer, where periodic management practices homogenize soil properties in agricultural areas, and (ii) that more process-related terrain attributes such as CA, the two indices WI and SPI, and the patterns of soil redistribution play a more important role in the spatial distribution of SOC in the deeper soil layers. The correlation between SOC and water erosion (SPI and E_{wat}) as well as between SOC and tillage erosion (E_{til}) indicates the importance of erosion and deposition in the deeper soil layers. The increasing correlations of SOC with CA and WI with increasing soil depth also points out that processes affecting soil moisture and infiltration influence the SOC patterns in these soil layers. The WI represents areas where water accumulates, and zones with higher WI values tend to have higher biomass production, lower SOC mineralization, and higher sediment deposition compared with zones of low WI (Terra et al., 2004).

In some respects our results disagree with other results where correlations between SOC and various primary terrain attributes were found. Mueller and Pierce (2003), for example, derived the highest correlation coefficients between SOC and elevation at

three different raster widths for the topsoil layer. They and other researchers (e.g., Terra et al., 2004; Takata et al., 2007) also found significant correlations with slope. The positive correlations with CA and WI correspond with the findings of other researchers (e.g., Terra et al., 2004; Sumfleth and Duttmann, 2008).

Soil Organic Carbon Kriging Results

For the high-density SOC input data, different combinations of theoretical variogram models and weighting methods performed best for the original SOC data in the three soil layers. Theoretical variogram parameters (Table 4) show that the original SOC data of R_{17} are moderately to highly spatially structured for all three soil layers, with low nugget/sill ratios. Ranges are much larger than the raster width, with a maximum value of 216 m for the SOC data in Soil Layer I, indicating that the sampling scheme used here accounts for most of the spatial variation of SOC in the three soil layers. The nugget variances comprising small-scale variability as well as measurement errors are close to zero in all soil layers. Mean errors calculated from cross-validation for OK in each soil layer are close to zero, indicating unbiased predictions (Table 4). Root mean square errors resulting from OK are 0.12, 0.20, and 0.15% (w/w) SOC for Soil Layers I, II, and III, respectively, corresponding to approximately 10, 28, and 44% of the mean SOC values in the different soil layers (Table 1). This indicates a loss of precision with increasing soil depth. In contrast, MEF is highest in Soil Layer III (MEF = 0.53) and lowest in Soil Layer II (MEF = 0.23). Plots of predicted vs. measured SOC contents (Fig. 4) show the greatest deviations from the 1:1 line in the case of Soil Layer II. The SOC maps derived from OK (Fig. 5) represent well the spatial distributions of SOC in each soil layer, which are already visible in the patterns of the measured SOC values at the sampling points (Fig. 2).

Regarding the theoretical variogram parameters of the residuals resulting from linear regression with the different significantly related covariables in the three soil layers (Table 4), the same conclusions as for the original SOC data in each soil layer can be drawn. The residuals are moderately or even highly spatially structured, and ranges are larger than the raster width. The sill of the different residual variograms is reduced compared with the sill of the raw data in all soil layers, reflecting the success of regression fitting (Hengl et al., 2004; Terra et al., 2004). Nugget variances are all close to zero.

In all three soil layers, the geostatistical interpolation of SOC could be improved by incorporating covariables in RK (Table 4). For Soil Layer I, there is only one covariable, namely C-prof. For Soil Layer II, C-prof, C-plan, CA, WI, and the three soil redistribution patterns derived from modeling were able to ameliorate the interpolation results, and in Soil Layer III improvements were achieved by using C-plan, CA_{tr}, SPI_{tr}, WI_{tr}, E_{til}, and E_{tot} as covariables in RK. Mean errors are still close to zero for all kriging approaches in all soil layers, indicating unbiased predictions. Due to the high spatial density of the original SOC data relative improvements of the described RK approaches compared to OK are only low to moderate in all three soil layers. In Soil Layers II and III, the integration of the more complex covariables outperformed that of the primary terrain parameters (Table 4). The improvement in Soil Layer III especially resulted from the more definite representation of high SOC contents situated in the depositional area at the downslope end of the test site (Fig. 4). In general, spatial distributions resulting from the best RK approach in each soil layer (Fig. 5) are similar to those derived from OK but show more small-scale variability.

Although a minimum number of at least 50 (better 100-150), sampling points is recommended for geostatistical analysis (Webster and Oliver, 2001), the theoretical semivariogram parameters of the SOC data and the values describing the goodness-of-fit for OK of the two reduced-input raster widths R_{25} (n = 92) and R_{50} (n = 44) still show reasonable results in each soil layer (Tables 5 and 6). As for the high-density sampling grid (R_{17}), different combinations of theoretical variogram models and weighting methods performed best for the original SOC data. Nugget/sill ratios show that the primary SOC data in the two subsoil layers are highly spatially structured in both raster widths, and SOC data in the topsoil are moderately spatially dependent. This indicates that the low-density sampling schemes are still suitable to resolve the spatial continuity of the original SOC data. For R_{25}, the ranges are larger than the raster width; only in Soil Layer II in R_{50} this is not the case. Nevertheless, the results of the R_{50} interpolation are still reasonable because the

Table 3. Quality of correlation between SOC content (% [w/w]) and all calculated parameters in the three soil layers (I: 0–0.25 m; II: 0.25–0.50 m; III: 0.50–0.90 m) expressed as Pearson correlation coefficients; results are given for the raster widths (R_{17}, 17.7 by 17.7 m; R_{25}, 25 by 25 m; R_{50}, 50 by 50 m) used as input for geostatistics.

Parameter†	Pearson correlation coefficient								
	R_{17} (n_I = 143, $n_{II,III}$ = 144)			R_{25} (n = 76)			R_{50} (n = 28)		
	I	II	III	I	II	III	I	II	III
RE, m	-0.04	-0.03	-0.28**	-0.16	-0.15	-0.31**	-0.37	-0.23	-0.45*
Slope, °	0.13	0.03	0.14	0.22	0.15	0.28*	0.26	0.15	0.37
Aspect, °	0.12	-0.01	0.08	0.28*	0.05	0.10	0.37	-0.12	0.04
C-prof, 0.01 m	0.37**	0.44**	0.39**	0.49**	0.47**	0.44**	0.53**	0.70**	0.55**
C-plan, 0.01 m	-0.28**	-0.36**	-0.56**	-0.38**	-0.34**	-0.44**	-0.46*	-0.45*	-0.52**
CA, m^2	0.19*	0.27**	0.67**	0.36**	0.46**	0.66**	0.48**	0.51**	0.65**
WI	0.14	0.35**	0.53**	0.08	0.37**	0.41**	0.24	0.48**	0.46*
SPI	0.25**	0.29**	0.67**	0.38**	0.43**	0.67**	0.53**	0.52**	0.71**
E_{til}, mm yr^{-1}	0.36**	0.45**	0.67**	0.48**	0.51**	0.57**	0.59**	0.59**	0.61**
E_{wat}, mm yr^{-1}	-0.22**	-0.25**	-0.53**	-0.25*	-0.32**	-0.50**	-0.51**	-0.45**	-0.68**
E_{tot}, mm yr^{-1}	0.33**	0.42**	0.55**	0.41**	0.41**	0.35**	0.47**	0.50**	0.40**

* Significant at 95%.

** Significant at 99%.

† Relative elevation (RE), slope, aspect, profile and plan curvature (C-prof and C-plan, respectively), catchment area (CA), wetness index (WI), stream power index (SPI), and patterns of tillage (E_{til}), water (E_{wat}), and total (E_{tot}) erosion.

Table 4. Theoretical semivariogram parameters of original soil organic C (SOC) data and residuals resulting from linear regression with different covariables as well as cross-validation results from ordinary (OK) and regression kriging (RK) of SOC content (% [w/w]) in three soil layers (I: 0–0.25 m; II: 0.25–0.50 m; III: 0.50–0.90 m) using the 17.7- by 17.7-m raster data set (R_{17}) (n_I = 159; $n_{II,III}$ = 160). The RK results are included only when they improve the prediction compared with OK. For exponential models, the practical range is given; goodness-of-fit was tested using mean error (ME), root mean square error (RMSE), model efficiency (MEF), and relative improvement (RI).

Soil layer	Covariable†	Theoretical semivariogram parameters						Kriging results			
		Model	Weight‡	Nugget	Sill	Range	Nugget/sill	ME	RMSE	MEF	RI
						m	%				%
I		exponential	equal	0.013	0.034	216	40	-0.001	0.123	0.45	–
	C-prof	exponential	equal	0.008	0.023	113	33	-0.002	0.115	0.53	6.50
II		exponential	$n_p h^{-2}$	0.000	0.054	40	0	-0.002	0.196	0.23	–
	C-prof	exponential	$n_p h^{-2}$	0.000	0.038	28	0	-0.001	0.192	0.26	2.04
	C-plan	exponential	$n_p h^{-2}$	0.000	0.047	35	0	-0.001	0.192	0.25	2.04
	CA	exponential	$n_p h^{-2}$	0.000	0.051	35	0	-0.002	0.194	0.24	1.02
	WI	exponential	$n_p h^{-2}$	0.000	0.050	36	0	-0.002	0.190	0.28	3.06
	E_{til}	exponential	$n_p h^{-2}$	0.000	0.039	28	0	-0.002	0.187	0.29	4.59
	E_{wat}	exponential	$n_p h^{-2}$	0.000	0.050	37	0	-0.002	0.195	0.24	0.51
	E_{tot}	exponential	$n_p h^{-2}$	0.000	0.040	29	0	-0.002	0.187	0.29	4.59
III		spherical	n_p	0.013	0.044	64	30	-0.002	0.145	0.53	–
	C-plan	spherical	n_p	0.011	0.030	64	37	-0.001	0.139	0.57	4.14
	CA_{tr}	spherical	n_p	0.008	0.037	79	23	-0.001	0.131	0.62	9.66
	WI_{tr}	spherical	n_p	0.010	0.041	87	24	-0.002	0.130	0.62	10.35
	SPI_{tr}	spherical	n_p	0.009	0.037	73	25	-0.000	0.136	0.59	6.21
	E_{til}	exponential	equal	0.000	0.024	22	0	-0.003	0.134	0.60	7.59
	E_{tot}	spherical	n_p	0.012	0.030	53	40	-0.002	0.134	0.60	7.59

† No covariable indicates OK was used; RK covariables are profile and plan curvature (C-prof and C-plan, respectively), catchment area (CA), wetness index (WI), stream power index (SPI), and patterns of tillage (E_{til}), water (E_{wat}), and total (E_{tot}) erosion. A subscript tr means that the values were transformed to logarithms so that linear regression residuals met normal distribution.

‡ Weighting of the semivariogram model was done by ordinary least squares (i.e., equal weights to all semivariances) and two weighted least square methods: weighting by n_p (number of pairs) and weighting by $n_p h^{-2}$ (h = lag distance [m]).

short distances formed by the transect and the two microplots were retained in each input raster. Nugget and sill variances of the original SOC data tended to be in the same order of magnitude as in R_{17} for each soil layer. Mean errors resulting from OK are still relatively low, indicating unbiasedness, and relations of the RMSEs to the mean values of the original SOC data also remain similar compared with the relations in R_{17} for each soil layer. Model efficiency through OK was 0.23 (R_{25}) and 0.14 (R_{50}) in Soil Layer I and 0.01 (R_{25}) and 0.15 (R_{50}) in Soil Layer II. Higher values for OK were again reached in the deepest soil layer, where an MEF of 0.34 (R_{25}) and 0.39 (R_{50}) was found. Deviations between measured and predicted SOC contents from the 1:1 line (Fig. 4) are similar for the two reduced raster widths compared with the high-density input grid, although a direct comparison between the different raster widths is not possible due to the use of different validation schemes.

The interpolated SOC distributions resulting from OK with the medium- and low-input data sets (Fig. 5) are smoothed compared with those using the high-density input data set in each soil layer. But even with coarse sampling (R_{50}), there is still a pronounced area with high SOC concentrations in the east in all soil layers. The second region with high SOC values (the southern edge and center), however, is no longer detectable in the R_{50} interpolation results for the deepest soil layer.

As was the case in R_{17}, nugget/sill ratios and the ranges of the various residuals for the different soil layers showed a moderate to high spatial structure. Sills were also lower than for the original SOC data, and nuggets were close to zero.

In contrast to the use of the high-resolution sampling grid R_{17} as input data, no improvements compared with OK were achieved in Soil Layer I by RK when using R_{25} and R_{50} (Tables 5 and 6). In Soil Layer II, RK including total erosion improved predictions best with R_{25} and R_{50} (RI = 8.4 and 6.2%, respectively). Relative improvements in Soil Layer III were even higher in the medium- and low-density raster than for Soil Layer II. In R_{25}, the spatial pattern of tillage erosion and in R_{50} the wetness index WI performed best in improving the RK results (Tables 5 and 6; Fig. 4).

In general, relative improvements in Soil Layers II and III using RK vs. OK were more pronounced in the case of medium- and low-density than high-density input data. Moreover, SOC maps produced by RK in Soil Layers II and III with R_{25} and R_{50} (Fig. 5) show considerably more detail and compare more favorably with the spatial patterns produced with R_{17} input data. Although a direct comparison of the interpolation results with the different input raster widths is not possible due to a missing independent data set, it has to be recognized that a reduction of input data density seems to slightly decrease MEF and increase RMSE.

Except for the high-density input data, our results for the topsoil layer agree with Terra et al. (2004), who found that OK predicted SOC best compared with cokriging, RK, and multiple regression for the uppermost 30 cm and for three different densities of input data (8, 32, and 64 samples ha^{-1}). In contrast, other researchers (e.g., Mueller and Pierce, 2003; Simbahan et al., 2006; Sumfleth and Duttmann, 2008) could improve the prediction of SOC in the topsoil layer by using (relative) elevation and electrical conductivity, respectively, as covariables in RK and kriging with external drift. Their studies showed that the sampling density played an important role in improving the performance of geostatistics when incorporating covariables. Mueller and Pierce (2003), for example, also used three different input raster widths at their test site. For their high-resolution input raster (10.7 samples ha^{-1}), they also found only modest

differences between the applied interpolation techniques, but for their two reduced raster widths (2.7 and 1 samples ha^{-1}), different interpolation methods incorporating covariables could outperform OK. This was also true for the three test sites of Simbahan et al. (2006) with sampling densities of 2.5 to 4.2 samples ha^{-1}. Our result of no or only slight improvements in the first soil layer might be caused by (i) our high sampling densities (38, 17, and 6 samples ha^{-1}), (ii) homogenization effects of management and the corresponding low spatial variability, and (iii) the area of high SOC concentrations at the southern boundary of the test site, which is most pronounced in the topsoil. The existence of this area cannot be ascribed to relief-driven processes, and in combination with homogenization it thus leads to relatively low correlations between SOC and the various parameters in the topsoil layer.

In contrast, considerable improvements of RK over OK in our study were achieved in the two subsoil layers. In Soil Layer II, this improvement was greatest when using the patterns of tillage or total erosion as a covariable in RK. This indicates that especially tillage-induced erosion and deposition processes affect the SOC distribution in this layer. This makes it necessary to consider not only water-induced soil redistribution processes, which are already represented in other primary and secondary terrain attributes (CA and SPI) used here and in other studies. Relative patterns of tillage erosion and deposition can easily be derived with well-tested erosion and sediment delivery models such as the WaTEM/SEDEM model. To implement the tillage erosion component, only a DEM and an estimation of the tillage transport coefficient are required (Van Oost et al., 2000).

Although the tillage and total erosion patterns significantly improved SOC prediction in the deepest soil layer for all three raster widths, comparable and in some instances even better results were produced by RK with CA and WI. This indicates that not only soil redistribution processes affect the spatial distribution of SOC in the deepest soil layer but also processes concerning the spatial distribution of infiltration and soil moisture. Both processes may increase SOC contents in the thalweg area due to (i) infiltration and absorption of dissolved organic C and (ii) limited mineralization of SOC in the case of high soil moisture contents.

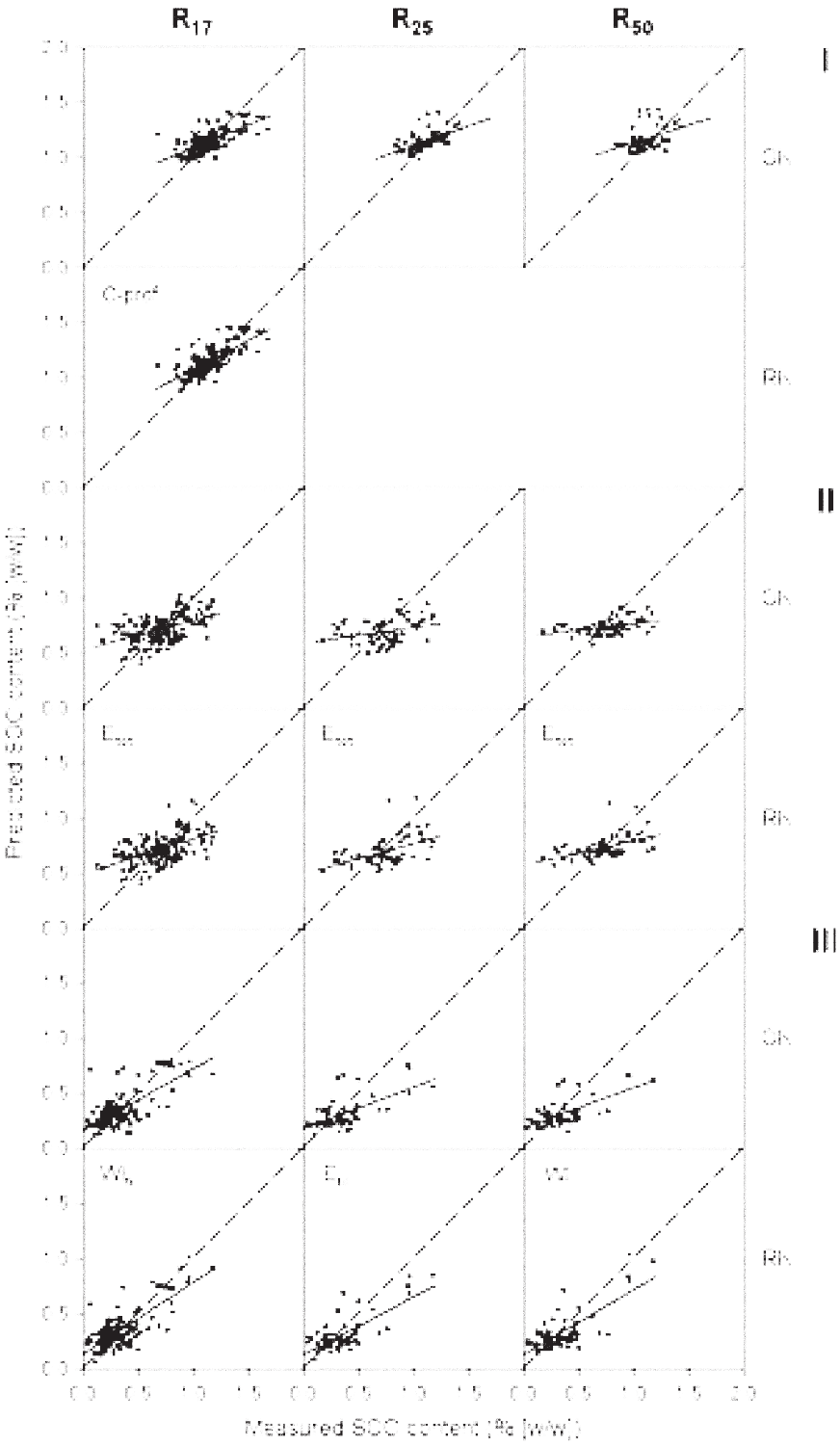

Fig. 4. Plots of predicted vs. measured soil organic C (SOC) contents (%w/w) for three soil layers (I: 0–0.25 m; II: 0.25–0.50 m; III: 0.50–0.90 m) resulting from ordinary (OK) and the best regression kriging (RK) approach using three different raster widths: R_{17} (17.7 by 17.7 m), R_{25} (25 by 25 m), and R_{50} (50 by 50 m) as input. Covariables of the RK approaches (profile curvature [C-prof], total erosion [E_{tot}], tillage erosion [E_{til}], and wetness index [WI]; WI_{tr} means that WI values were transformed to logarithms so that linear regression residuals met normal distribution) are given in each plot; the 1:1 line is dashed, linear regression fit is indicated by a solid line.

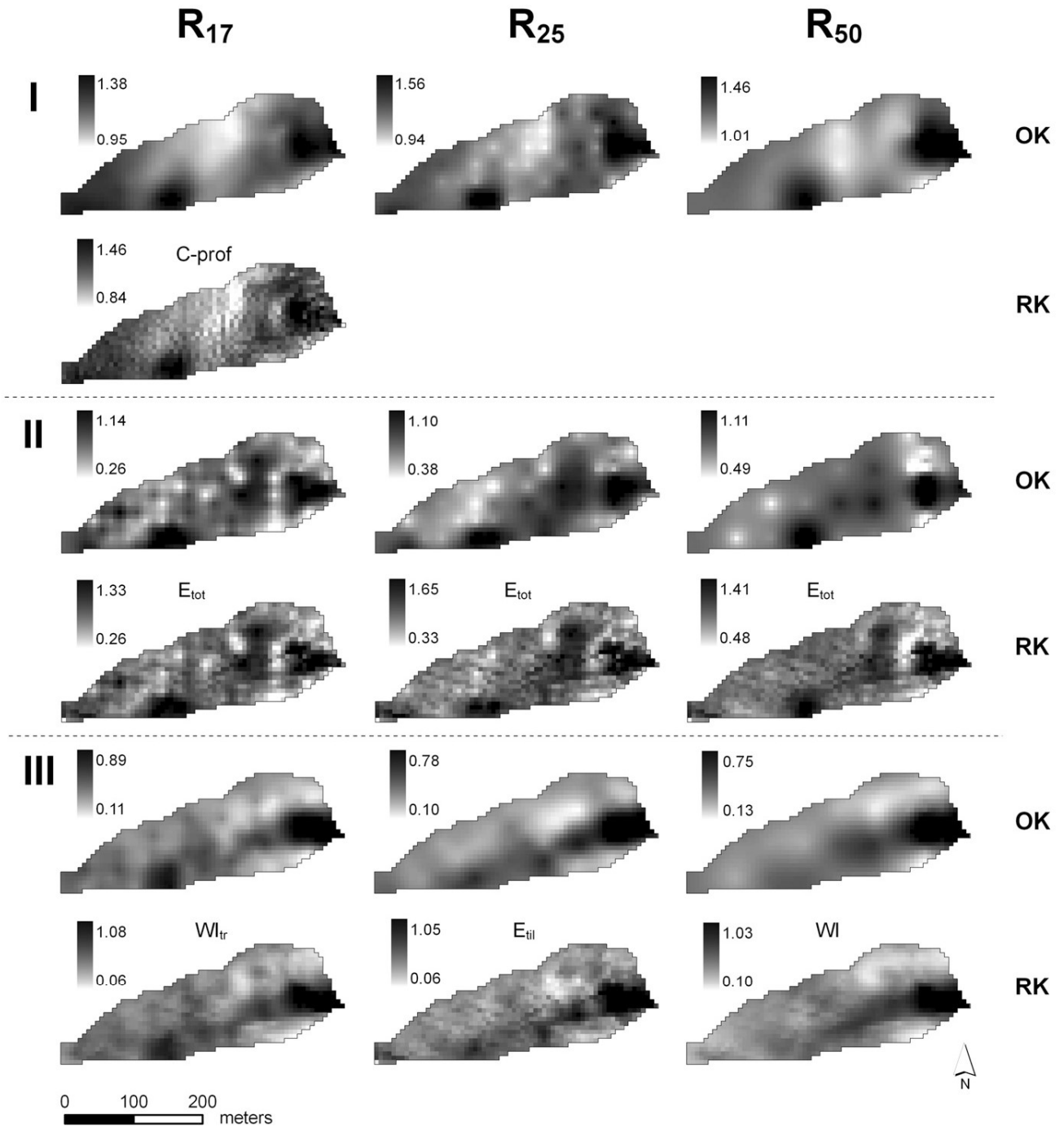

Fig. 5. Maps of soil organic C content (% [w/w]) for three soil layers (I: 0–0.25 m; II: 0.25–0.50 m; III: 0.50–0.90 m) resulting from ordinary (OK) and the best regression kriging (RK) approach using three different raster widths: R_{17} (17.7 by 17.7 m), R_{25} (25 by 25 m), and R_{50} (50 by 50 m) as input. Covariables of the RK approaches (profile curvature [C-prof], total erosion [E_{tot}], tillage erosion [E_{til}], and wetness index [WI]; WI_{tr} means that WI values were transformed to logarithms so that linear regression residuals met normal distribution) are given above each map.

In contrast to the topsoil layer, in the two subsoil layers, improved SOC interpolations were actually obtained when using a high density of input data for RK. This was possibly caused by higher spatial variations of SOC in these soil layers, expressed as the coefficient of variation (Table 1).

CONCLUSIONS

Our results show that the spatial SOC patterns in a sloped arable test site differ significantly among three soil layers. Whereas the topsoil SOC pattern was homogenized by tillage operations, the patterns of the two subsoil layers show an increasing spatial variability primarily caused by high SOC contents in the depositional area at the downslope end of the test site. In the middle soil layer (0.25–0.50 m), the best RK result was produced with the patterns of tillage and total erosion, indicating the importance of soil redistribution (especially the inclusion of tillage erosion) for the spatial distribution of SOC in agricultural areas. In the third soil layer (0.50–0.90 m), tillage and total erosion as

Table 5. Theoretical semivariogram parameters of original soil organic C (SOC) data and residuals resulting from linear regression with different covariables as well as results from ordinary (OK) and regression kriging (RK) with SOC content (% [w/w]) in three soil layers (I: 0–0.25 m; II: 0.25–0.50 m; III: 0.50–0.90 m) using the 25- by 25-m raster data set (R_{25}) (n = 92). The values describing the goodness-of-fit result from the comparison with a validation data set (n = 67); RK results are included only when they improve the prediction compared with OK. For exponential models the practical range is given; goodness-of-fit was tested using mean error (ME), root mean square error (RMSE), model efficiency (MEF), and relative improvement (RI).

Soil layer	Covariable†	Theoretical semivariogram parameters						Kriging results			
		Model	Weight‡	Nugget	Sill	Range	Nugget/sill	ME	RMSE	MEF	RI
						m	%				%
I		exponential	equal	0.003	0.035	41	9	-0.033	0.118	0.23	–
II		exponential	$n_p h^{-2}$	0.000	0.052	40	0	0.058	0.226	0.01	–
	WI	exponential	$n_p h^{-2}$	0.000	0.050	37	0	0.049	0.217	0.09	3.98
	E_{til}	spherical	n_p	0.006	0.029	34	20	0.055	0.221	0.06	2.21
	E_{wat}	exponential	$n_p h^{-2}$	0.000	0.047	31	0	0.058	0.223	0.04	1.33
	E_{tot}	exponential	$n_p h^{-2}$	0.000	0.031	25	0	0.053	0.207	0.17	8.40
III		spherical	equal	0.010	0.044	56	23	0.053	0.181	0.34	–
	C-plan	spherical	$n_p h^{-2}$	0.001	0.032	57	3	0.053	0.171	0.41	5.55
	CA_{tr}	spherical	equal	0.006	0.040	65	16	0.048	0.159	0.50	12.15
	WI_{tr}	spherical	equal	0.016	0.044	67	26	0.047	0.159	0.48	12.15
	SPI_{tr}	spherical	equal	0.006	0.037	57	17	0.051	0.167	0.43	7.73
	E_{til}	exponential	$n_p h^{-2}$	0.000	0.027	53	0	0.054	0.158	0.50	12.71
	E_{wat}	spherical	equal	0.013	0.037	66	35	0.053	0.172	0.40	4.97
	E_{tot}	spherical	equal	0.015	0.034	70	44	0.050	0.159	0.49	12.15

† No covariable indicates OK was used; RK covariables are plan curvature (C-plan), catchment area (CA), wetness index (WI), stream power index (SPI), and patterns of tillage (E_{til}), water (E_{wat}), and total (E_{tot}) erosion. A subscript tr means that the values were transformed to logarithms so that linear regression residuals met normal distribution.

‡ Weighting of the semivariogram model was done by ordinary least squares (i.e., equal weights to all semivariances) and two weighted least square methods: weighting by n_p (number of pairs) and weighting by $n_p h^{-2}$ (h = lag distance [m]).

well as the WI and partly the CA performed best. This indicates that besides soil redistribution, also processes concerning the distribution of soil moisture affect the spatial pattern of SOC in the deepest soil layer. Here SOC contents in the depositional area were as high as topsoil SOC contents, indicating the importance of including deeper soil layers when assessing soil C balances, especially in hilly agricultural areas.

Because patterns of topsoil SOC distribution might be dissimilar to subsoil patterns, particularly in agricultural areas prone to soil erosion and deposition, estimating total SOC pools from topsoil SOC, for instance by applying remote sensing techniques (e.g., Stevens et al., 2008), might not be appropriate.

In general, it was shown that (especially) integrating patterns of soil redistribution (which must include tillage erosion) in kriging approaches can substantially improve SOC interpolation of subsoil data in hilly arable landscapes. This is an important finding insofar as high-resolution subsoil SOC data are rare and

Table 6. Theoretical semivariogram parameters of original soil organic C (SOC) data and residuals resulting from linear regression with different covariables as well as results from ordinary (OK) and regression kriging (RK) of SOC content (% [w/w]) in three soil layers (I: 0–0.25 m; II: 0.25–0.50 m; III: 0.50–0.90 m) using the 50- by 50-m raster data set (R_{50}) (n = 44). The values describing the goodness-of-fit result from the comparison with a validation data set (n = 67); RK results are included only when they improve the prediction compared with OK. For exponential models, the practical range is given. Goodness-of-fit was tested using mean error (ME), root mean square error (RMSE), model efficiency (MEF), and relative improvement (RI).

Soil layer	Covariable†	Theoretical semivariogram parameters						Kriging results			
		Model	Weight‡	Nugget	Sill	Range	Nugget/sill	ME	RMSE	MEF	RI
						m	%				%
I		spherical	n_p	0.014	0.047	75	30	-0.055	0.139	0.14	–
II		exponential	$n_p h^{-2}$	0.000	0.060	48	0	0.015	0.210	0.15	–
	C-prof	exponential	$n_p h^{-2}$	0.000	0.019	15	0	0.015	0.206	0.18	1.90
	E_{til}	spherical	n_p	0.011	0.029	48	41	0.019	0.202	0.20	3.81
	E_{tot}	spherical	n_p	0.012	0.029	50	40	0.015	0.197	0.25	6.19
III		spherical	n_p	0.007	0.071	79	10	0.046	0.174	0.39	–
	WI	spherical	n_p	0.010	0.070	75	14	0.028	0.149	0.55	14.37
	E_{til}	spherical	n_p	0.012	0.045	76	27	0.041	0.158	0.49	9.20
	E_{tot}	spherical	equal	0.018	0.050	84	36	0.040	0.162	0.47	6.90

† No covariable indicates OK was used; RK covariables are profile curvature (C-prof), wetness index (WI), and patterns of tillage (E_{til}) and total (E_{tot}) erosion.

‡ Weighting of the semivariogram model was done by ordinary least squares (i.e., equal weights to all semivariances) and two weighted least square methods: weighting by n_p (number of pairs) and weighting by $n_p h^{-2}$ (h = lag distance [m]).

the promising approach to improving spatial estimates of SOC by applying remote sensing techniques is limited to topsoil SOC.

ACKNOWLEDGMENTS

The study was carried out in the framework of the German Research Agency (DFG) project "Soil redistribution in agricultural landscapes—source or sink of CO_2?" FI 1216/4-1. The assistance with field work and geostatistics in GNU R by Christian Koyama and Paul Wagner is gratefully acknowledged. Special thanks also go to the farm owner Phillip Töllner for his permission to carry out several field campaigns and his patience in answering field management questions.

REFERENCES

Ahmed, S., and G. De Marsily. 1987. Comparison of geostatistical methods for estimating transmissivity using data on transmissivity and specific capacity. Water Resour. Res. 23:1717–1737.

Arriaga, F.J., and B. Lowery. 2005. Spatial distribution of carbon over an eroded landscape in southwest Wisconsin. Soil Tillage Res. 81:155–162.

Beven, K.J., and M.J. Kirkby. 1979. A physically based, variable contributing area model of basin hydrology. Hydrol. Sci. Bull. 24:43–69.

Cambardella, C.A., T.B. Moorman, J.M. Novak, T.B. Parkin, D.L. Karlen, R.F. Turco, and A.E. Konopka. 1994. Field-scale variability of soil properties in central Iowa soils. Soil Sci. Soc. Am. J. 58:1501–1511.

Chai, X., C. Shen, X. Yuan, and Y. Huang. 2008. Spatial prediction of soil organic matter in the presence of different external trends with REML-EBLUP. Geoderma 148:159–166.

Chen, F., D.E. Kissel, L.T. West, and W. Adkins. 2000. Field-scale mapping of surface soil organic carbon using remotely sensed imagery. Soil Sci. Soc. Am. J. 64:746–753.

Desmet, P.J.J., and G. Govers. 1996. A GIS procedure for automatically calculating the USLE LS factor on topographically complex landscape units. J. Soil Water Conserv. 51:427–433.

Deutsches Institut für Normung. 1996. DIN 18129:1996-11. Baugrund, Untersuchung von Bodenproben- Kalkgehaltsbestimmung. Beuth Verlag, Berlin.

Deutsches Institut für Normung. 2005. DIN 19708. Bodenbeschaffenheit: Ermittlung der Erosionsgefährdung von Böden durch Wasser mit Hilfe der ABAG. Beuth Verlag, Berlin.

Govers, G., T.A. Quine, and D.E. Walling. 1993. The effect of water erosion and tillage movement on hillslope profile development: A comparison of field observation and model results. p. 285–300. *In* S. Wicherek (ed.) Farm land erosion in temperate plains environments and hills. Elsevier, Amsterdam.

Govers, G., K. Vandaele, P. Desmet, J. Poesen, and K. Bunte. 1994. The role of tillage in soil redistribution on hillslopes. Eur. J. Soil Sci. 45:469–478.

Hengl, T., G.B.M. Heuvelink, and D.G. Rossiter. 2007. About regression-kriging: From equations to case studies. Comput. Geosci. 33:1301–1315.

Hengl, T., G.B.M. Heuvelink, and A. Stein. 2004. A generic framework for spatial prediction of soil variables based on regression-kriging. Geoderma 120:75–93.

Herbst, M., B. Diekkrüger, and H. Vereecken. 2006. Geostatistical co-regionalization of soil hydraulic properties in a micro-scale catchment using terrain attributes. Geoderma 132:206–221.

Isaaks, E.H., and R.M. Srivastava. 1989. Applied geostatistics. Oxford Univ. Press, New York.

Kerry, R., and M.A. Oliver. 2007a. Determining the effect of asymmetric data on the variogram: I. Underlying asymmetry. Comput. Geosci. 33:1212–1232.

Kerry, R., and M.A. Oliver. 2007b. Determining the effect of asymmetric data on the variogram: II. Outliers. Comput. Geosci. 33:1233–1260.

Lark, R.M., B.R. Cullis, and S.J. Welham. 2006. On spatial prediction of soil properties in the presence of a spatial trend: The empirical best linear unbiased predictor (E-BLUP) with REML. Eur. J. Soil Sci. 57:787–799.

Mabit, L., C. Bernard, M. Makhlouf, and M.R. Laverdière. 2008. Spatial variability of erosion and soil organic matter content estimated from ^{137}Cs measurements and geostatistics. Geoderma 145:245–251.

Matheron, G. 1963. Principles of geostatistics. Econ. Geol. 58:1246–1266.

Minasny, B., and A.B. McBratney. 2007a. Spatial prediction of soil properties using EBLUP with the Mátern covariance function. Geoderma 140:324—336.

Minasny, B., and A.B. McBratney. 2007b. Corrigendum to "Spatial prediction of soil properties using EBLUP with the Mátern covariance function" [Geoderma 140 (2007) 324–336]. Geoderma 142:357–358.

Moore, I.D., P.E. Gessler, G.A. Nielsen, and G.A. Peterson. 1993. Soil attribute prediction using terrain analysis. Soil Sci. Soc. Am. J. 57:443–452.

Mueller, T.G., and F.J. Pierce. 2003. Soil carbon maps: Enhancing spatial estimates with simple terrain attributes at multiple scales. Soil Sci. Soc. Am. J. 67:258–267.

Mueller, T.G., F.J. Pierce, O. Schabenberger, and D.D. Warncke. 2001. Map quality for site-specific fertility management. Soil Sci. Soc. Am. J. 65:1547–1558.

Mueller, T.G., N.B. Pusuluri, K.K. Mathias, P.L. Cornelius, and R.I. Barnhisel. 2004. Site-specific soil fertility management: A model for map quality. Soil Sci. Soc. Am. J. 68:2031–2041.

Nash, J.E., and J.V. Sutcliffe. 1970. River flow forecasting through conceptual models: I. A discussion of principles. J. Hydrol. 10:282–290.

Odeh, I.O.A., A.B. McBratney, and D.J. Chittleborough. 1994. Spatial prediction of soil properties from landform attributes derived from a digital elevation model. Geoderma 63:197–214.

Odeh, I.O.A., A.B. McBratney, and D.J. Chittleborough. 1995. Further results on prediction of soil properties from terrain attributes: Heterotopic cokriging and regression-kriging. Geoderma 67:215–226.

Pebesma, E.J. 2004. Multivariable geostatistics in S: The gstat package. Comput. Geosci. 30:683–691.

Ping, J.L., and A. Dobermann. 2006. Variation in the precision of soil organic carbon maps due to different laboratory and spatial prediction methods. Soil Sci. 171:374–387.

Quinn, P., K. Beven, P. Chevallier, and O. Planchon. 1991. The prediction of hillslope flow paths for distributed hydrological modelling using digital terrain models. Hydrol. Processes 5:59–79.

R Development Core Team. 2007. R: A language and environment for statistical computing. R Foundation for Statistical Computing, Vienna.

Renard, K.G., G.R. Foster, G.A. Weesies, D.K. McCool, and D.C. Yoder. 1996. Predicting soil erosion by water: A guide to conservation planning with the Revised Universal Soil Loss Equation (RUSLE). Agric. Handbk. 703. U.S. Gov. Print. Office, Washington, DC.

Ritchie, J.C., G.W. McCarty, E.R. Venteris, and T.C. Kaspar. 2007. Soil and soil organic carbon redistribution on the landscape. Geomorphology 89:163–171.

Schäuble, H. 2004. HydroTools 1.0 for ArcView 3.x. TERRACS, Tübingen, Germany.

Schlesinger, W.H. 2005. The global carbon cycle and climate change. Adv. Econ. Environ. Resour. 5:31–53.

Simbahan, G.C., A. Dobermann, P. Goovaerts, J. Ping, and M.L. Haddix. 2006. Fine-resolution mapping of soil organic carbon based on multivariate secondary data. Geoderma 132:471–489.

Soil Survey Staff. 1999. Soil Taxonomy: A basic system of soil classification for making and interpreting soil surveys. 2nd ed. U.S. Gov. Print. Office, Washington, DC.

Stevens, A., B. van Wesemael, H. Bartholomeus, D. Rosillon, B. Tychon, and E. Ben-Dor. 2008. Laboratory, field and airborne spectroscopy for monitoring organic carbon content in agricultural soils. Geoderma 144:395–404.

Sumfleth, K., and R. Duttmann. 2008. Prediction of soil property distribution in paddy soil landscapes using terrain data and satellite information as indicators. Ecol. Indic. 8:485–501.

Takata, Y., S. Funakawa, K. Akshalov, N. Ishida, and T. Kosaki. 2007. Spatial prediction of soil organic matter in northern Kazakhstan based on topographic and vegetation information. Soil Sci. Plant Nutr. 53:289–299.

Terra, J.A., J.N. Shaw, D.W. Reeves, R.L. Raper, E. van Santen, and P.L. Mask. 2004. Soil carbon relationships with terrain attributes, electrical conductivity, and a soil survey in a Coastal Plain landscape. Soil Sci. 169:819–831.

Van Oost, K., G. Govers, and P. Desmet. 2000. Evaluating the effects of changes in landscape structure on soil erosion by water and tillage. Landscape Ecol. 15:577–589.

Van Rompaey, A.J.J., G. Verstraeten, K. Van Oost, G. Govers, and J. Poesen. 2001. Modelling mean annual sediment yield using a distributed approach. Earth Surf. Processes Landforms 26:1221–1236.

Verstraeten, G., J. Poesen, K. Gillijns, and G. Govers. 2006. The use of riparian vegetated filter strips to reduce river sediment loads: An overestimated control measure? Hydrol. Processes 20:4259–4267.

Verstraeten, G., K. Van Oost, A. Van Rompaey, J. Poesen, and G. Govers. 2002. Evaluating an integrated approach to catchment management to reduce soil loss and sediment pollution through modelling. Soil Use Manage. 19:386–394.

Webster, R., and M.A. Oliver. 2001. Geostatistics for environmental scientists. John Wiley & Sons, Chichester, UK.